Guardiola, J., Elvira, R. & Briongos, J. (2020). Superficial oscillation as an identifier of phenomena governing dynamics of solid–gas fluidized systems. *Powder Technology*, 362, pp. 770–780.

DOI: 10.1016/j.powtec.2019.12.009

Superficial oscillation as an identifier of phenomena governing dynamics of solid–gas fluidized systems

J. Guardiola[1]

University of Alcala, Department of Chemical Engineering, Edificio Polivalente Campus, 28871 Alcalá de Henares, Madrid, Spain

R. Elvira

University Nebrija of Madrid, Departamento Ingeniería Industrial y Automoción, Escuela Politécnica Superior, Pirineos, 55. 28040 Madrid, Spain

J.V. Briongos,

Universidad Carlos III de Madrid. Escuela Politécnica Superior. Departamento de Ingeniería Térmica y de Fluidos, Avenida de la Universidad 30, 28911, Leganés (Madrid)

Abstract

The evolution of the volume of a fluidized bed solid–gas over time is measured by the oscillation of its surface. It is assumed that the system is governed by the pressure gradient between the plenum and the surface; the latter is considered as the reference.

The surface oscillation is measured with a laterally located CCD video camera such that it monitors the flattest portion of the surface and records its coordinates. Simultaneously obtain all the phenomena that regulate the hydrodynamics of the bed, the entering bubbles, coalesce, split, increase their volume adiabatically, and explode on the surface. The gas flow and the weight of fluidized material are studied. The time series of the surface oscillation is analysed in the frequency domain and the phase space. The frequencies obtained are approximately between 0.6 Hz and 1.8 Hz. The entropy values behaves linearly proportional to the total number of bubbles.

[1] Corresponding author: phone +34 91 8854976; jesus.guardiola@uah.es

1 Introduction

The fluidized bed (FB) can be seen it a flow retention device comprising two components; one of these is rigid (a perforated plate), and the other component is dynamical (a bed of interacting solid particles). The perforate plate distributes the fluid and supports the particles; therefore, it is located at the bottom. The system operates because it is subject to a pressure gradient; the pressure on the upper surface of the bed (generally, the atmospheric pressure) can be taken as the pressure reference point. As a result the good mass and heat transfer properties of FB's facilitate the interaction between the phases and explains its use in industry to act as catalytic reactor, granulator, dryer, or boiler generating energy from fossil fuels.

The characterization of fluidized bed dynamics have drawn the research effort of a broad number of researchers trying to understand the physics of the dynamics behind the measured signals. Thus, the first attempts focus on properties likely to be measured and which where apparently global dynamic bed properties such as the frequency of the pressure fluctuation measured in the plenum were analysed using statistical and frequency analysis tools. Although numerous authors have measured it [1, 2], it is not fairly global property because it could miss information regarding the interactions and growing mechanism of the bubbles inside the bed. Accordingly, the pressure in the plenum should oscillate because of bubble generation process and the pressure fluctuation resulting from the pressure gradient between the distributor and the upper surface. Moreover, there are a huge literature that uses local in-bed measures such as pressure fluctuation, capacity and electrical resistance measurement to information about the number and size of bubbles and bubble behaviour Cheremisinoff [3], Geldart [4], Werther [5], van Ommen et al. [6], Aghbashlo et al. [7], and Sun et al. [8].

This research is focused on monitoring the long term behaviour of fluidized beds. Accordingly, the fluidization process can be seen it as phenomenon governed by the pressure gradients that can be affected by the diameter and velocity of the bubbles, driving the dynamics of the system. In order to measure the variation in bed volume over time, the fluctuations of the bed surface have been collected from a FB system consisting of a 2D solid–gas fluidized bed and a computer vision solution for laterally inspecting the surface of the bed [9, 10]. The measured system used is both global and adaptive, since it is able to adjust the measurement area to sift out the bubble bursting component from the top surface fluctuation measure. The subsequent time series analysis are in agreement with previous results report in literature but lacks of spurious information originated by the local bubble bursting phenomena.

1.1.1 Tools to analyse the time series of bed height

According to the interpretation of the FB that has been proposed, the analysis in the frequency domain and in the state space should be used as the tools.

1.1.2 Frequency domain

This analysis is carried out using the Fourier transform and is aimed at obtaining the dominant frequencies present in the time series and assigning them to the several physical phenomena. This analysis has also been applied to identify fluidization regimes comparing normalized power spectra [11-13], to investigate the dynamics of bubbles [14,15] and to monitor in real time the beds' hydrodynamics [16].

1.1.3 State space analysis

Numerous authors have explained the low-dimensional dynamics that gas–solid fluidized systems apparently exhibit, using state space analysis. This method of analysis first reconstructs the attractors in an embedded phase space and then measures the properties of the attractor, such as the correlation dimension and the Kolmogorov entropy (KE). In addition, the state space analysis has been successfully applied in several fields of fluidization engineering such as modelling [17], control [18, 19], and scale-up [20].

Correlation dimension

It represents the spatial unit of measurement of the attractor, D_2, and it is obtained by calculating the spatial correlation between random points on the reconstructed attractor. It was proposed by Grassberger and Procaccia [21]. Subsequently, other researchers described calculation methods based on the aforementioned authors work [22-23]. In our case, the attractor is first reconstructed in an embedding dimension equal to 10 previously selected through a false neighbour analysis [24]; a time delay of one was also used, and the interpoint distance was computed using the maximum norm [25].

Kolmogorov entropy

Given the method to construct and represent the attractor, whereas D_2 is the spatial unit of the attractor, the KE is the temporal unit. Thus, this parameter measures the average degree of uncertainty one experiences by making a new measurement, in spite of availability of knowledge of its history [26]. It expresses the effect that several past measurements exert on the current measure and reflects the rate of information loss by the system (unpredictability). That's why when dealing with periodic, completely deterministic data, KE is equal to zero, when the character of time series is random the entropy is infinite and consequently, deterministic chaotic

phenomena exhibit a positive KE. There are several methods to estimate KE from experimental time series [26, 27] ; the method used here is based on the maximum likelihood method [28].

2 Experimental apparatus and operating procedure

The experimental set up has been described elsewhere [9,10]. Briefly, the system consists of a 2D solid–gas fluidized bed and a computer vision system for laterally inspecting the surface of the bed (Figure 1).

Glass ballotini of 420–500 μm and ρ_p = 2630 kg/m^3 was fluidized with air at ambient conditions and 60 % moisture in order to prevent the formation of electric charge by friction with the surface of the column. The gas fluidization was measured by a set of three rotameters and its humidity by a hygrometer (Testo 635). The column was made of methyl methacrylate, 1.0 (height) × 0.2 (width) × 0.009 (depth) m; it had a perforated plate distributor with orifices of 3 × 10^{-4} m$^{\Phi}$, which give an open area of 0.28%. The weights and gas flow of fluidization are presented in Table 1.

The computer vision system was a CCD video camera that could be moved vertically by means of a positioning system (PS). The CCD camera used was a Sony XC-75CE with a sensing element of 582 (horizontal dimension) × 752 (vertical dimension) pixels; the size of each pixel was 8.6 × 8.3 μm. A strobe lighting device (LD), which operated in synchrony with the camera, illuminated the back of the bed. The camera was laterally to the bed placed, 0.36 m. It could monitor a surface such as the ABCD area in the figure whose measure unit is P_x = 216 μm and P_y = 208 μm. The capture velocity is 25 images/s, and the images are binarized at a threshold that can be selected manually or automatically. The CCD was connected to a PC that regulated its operation using customized software.

The PS has the purpose of enabling the CCD to permanently "see" the surface of the bed; it was focused laterally. For a specific static bed height and fluidization rate, the surface will preferably oscillate in a certain region; therefore, the CCD is previously placed in the optimal position so that all the values attained by the height enter within its field of vision. This is achieved with an automated RoboCylinder ERC-SA6, which is connected to a PC and can move the camera at a velocity 0.001–0.100 m/s with a stroke of 0.45 m and a resolution of 10^{-5} m.

The objective of the software that regulated the CCD was to make the vision system to examine the FB–air interface; that is, when it inspected the upper surface of the bed, it identified the best horizontal segment and recorded its position. This was performed using a pattern rectangle whose area was split horizontally into two regions: the upper one with clear pixels and the lower

one with dark pixels; it constantly examined the ABCD view field, searching for the region that most closely matched the pattern.

Briefly, the operation procedure was as follows:

1) Pattern generation: its dimensions, namely, width and height ($w \times h$) are decided and introduced by the software; the image of the corresponding rectangle appears on the monitor.
2) The ratio between the upper and lower regions of the pattern (light/dark pixels; e.g., 40/60) were decided and introduced by the software.
3) Maintaining the bed static, the CCD was shifted to a position such that the bed was visible according to the determined ratio, and the image was recorded.
4) Measured the bed height over time: the bed was fluidized, and during the experiment, which consumed 27 min (equivalent to 40 000 data), the region of the bed that best matched the pattern was captured. The position coordinates of this bed region and the degree of pattern matching were recorded at the established frequency (25 Hz).

More specific handling details can be observed in the two aforementioned items [15, 35].

The most preferred facilities for hydrodynamic measurements of fluidized systems are 3D cylindrical beds. However, to improve the capture of surface oscillation, we decided to slow down the phenomenon operating with 2D beds. In these beds, the generation, coalescence, splitting, and explosion of bubbles continue even when the dynamics of bubbles was slowed by the friction with the walls.

3 Results and discussion

The variation in the bed volume, measured as height, for different operating conditions are presented in Figures 2 and 3; they illustrate the effects of the gas flow and the weight of fluidized material, respectively. It is observed that in all the cases, the time signal includes the repetitive phenomenon of the entrance/exit of the bubbles and the irregularities that represent the coalescence, splitting, and adiabatic expansion of the bubbles. Therefore, the signal was analysed in the frequency domain and in the phase space.

3.1 Analysis in the frequency domain

The power spectral density function was obtained from FFT analysis of the data of height fluctuation over time; the spectra obtained are shown in Figure 4. Previously, to verify that the

FFT was representative of the trial, the calculation was performed for different samples of 1024 data extracted at random from throughout the time series, and the results were compared with each other; in all the cases, the values of the main frequency, F_P, were fairly close (standard deviation/mean)$_{Fp}$ < 3.0%, when the calculation was repeated 10 times. The figure shows that F_P decreased from (a) to (c) (1.53, 1.09, and 0.65 Hz, respectively); this in turn corresponds to an increase in height or its equivalent the bed weight, and a decrease in the fluidization gas. In conclusion, at least one of the two variables influenced the phenomenon.

The reduction in blur of the spectrums from (a) to (c) could be because u_f (and therefore the agitation) decreases. Assuming that the main frequency represented the oscillation of the bed surface and considering that the height in case (a) was small (i.e., the phenomena occurring in the distributor were detected on the surface), the second main frequency shown in (a) could represent the bubble inlet to the bed. In (c), another second main frequency appears, which could represent the incipient slugging produced because now, L/D was higher than those for the other two cases considered.

The values of the first F_P depending on W and u_f are shown in Figure 5; it is observed that

1) The frequency of bed volume variation increased marginally with increase in the flow of the fluidization gas when the weight of fluidized material was constant. This is shown in Figure 2 for four specific cases; the figure shows that when the flow (or the fluidizing gas pressure that caused it) increased, the entry/exit of bubbles accelerated. Furthermore, Figure 2 shows that for experiments (a) and (b) that were carried out with an identical quantity of particles, case (b) exhibited a marginally higher frequency, a larger amplitude (i.e., the size of the bubbles is larger), and a higher most probable height; this implies that the holdup increased. In the same figure, experiments (c) and (d) exhibit a behaviour similar as that of (a) and (b).
2) The frequency decreased with increase in the weight of the fluidized material when the flow rate was constant (Figure 5). The phenomenon, which is illustrated in detail in Figure 3, could be explained considering that the distance and time bubble ascension from the distributor to the surface increased. The figure also that the amplitude (size of bubbles) is similar, which could be because when the weight was increased, the pressure in the holes distributor increased and the formation size, d_{b0}, decreased. That is, the sizes were similar because the largest increase in volume by adiabatic expansion offset the lower d_{b0}.

The observed similar effects on the bed weight and fluidization velocity on the frequency has been previously reported in literature by Kage et al. [29,30], Lirag et al. [1], and Fan et al. [2]

from pressure fluctuation signals collected in the plenum and in various positions within the bed. However, it is worth to point out that in contrast to pressure fluctuation signals, in this research the dynamic behind the collected time series is clearly identified.

3.2 Analysis in the phase space

As mentioned previously, the suitable analysis tool of the state space is the attractor because it contains the dynamics of the phenomenon. Before the attractors were reconstructed, the data was re-escalated by applying the singular value decomposition (SVD) or principal component analysis.

The spectrum of eigenvalues for different experimental conditions when the gas velocity and quantity of fluidized material changed is shown in Figures 6 and 7, respectively. For all these, background noise appeared for embedding dimensions larger than 4–6. In the first case, with *W* constant (Figure 6), there was a marginal increase (from 4 to 6) in the values of the variables containing the dynamics when the flow of the fluidizing gas was increased. Moreover, when the static bed height increased from 292.87 mm to 443.70 mm (Figure 7), the background noise is reached earlier, changing the aforementioned variables from 5 to 4. Thus, the number of degrees of freedom of the phenomenon was similar for all the experiments although the behaviour of the fluidized system remains, the fluidization conditions favours the formation of bubbles, their collisions and the explosion on the surface, whereas the increase in the *L*/*D* ratio originated the well-known tendency to form slugs. These results agree with those of several authors and indicate that most of the information remains in the first two or three axes.

The attractors represented in the space of three components are presented in Figure 8. It is observed that when the velocity is low, its geometry resembles that of a "boat" whereas the aspect is inverted when the gas flow increases. As expected, the size of the space occupied by the attractor also grows moderately as the flow increases; this is apparent from the axis scales. Case (a) is for velocity marginally higher than the minimum fluidization (u_{mf} = 0.418 cm/s). The reason is that higher gas flow lead to larger erupting bubbles and consequently, there is an increase in the amplitude of the measured signals (Figure 2). Figure 9 shows another series for a larger weight of fluidized material (1.567 kg). The trend is similar to the previous one, and it is apparent that the space occupied by the attractors of the second series was moderately larger than the first.

More conventional is to analyse the two principal components resulting from the SVD decomposition, i.e., in the 2D plane, the effect of the bed weight is also apparent. Thus, the function PC2 vs. PC1 in Figure 10a resembles an arrowhead to the right with the end at the origin

of the PC2 scale; subsequently, when it evolved according to the conditions of (b) and (d), the figure appears to have rotated in the clockwise direction, as a result of rising the gas flow and consequently promote a more uniform fluidization conditions. It can be observed that the aforementioned arrowhead passes to the lower right part of the plane PC2 vs. PC1.

Correlation dimension

As mentioned earlier, a method to measure the attractor is to determine D_2. Its evolution with the fluidization gas flow rate when the bed was bubbling is presented in Figure 11a. It is observed that D_2 grew from 1–3 for flows moderately higher than u_{mf} (for this material is 0.422 m/s- up to 4.0-4.5 while it was in clear bubbling. Figures 12a–d shows that for higher values of the *L*/*D* ratio, once complete bubbling was attained, the dimension was maintained in a range of values close to 4.0. This is in agreement with the attractor size predicted by the eigenvalue analysis. In all the cases, before the correlation dimension attained the quasi-constant value, there was a flow range in which visual observation revealed isolated bubbling, which was approximately 10% above the u_{mf} for both *L*/*D* lower, and narrower for the three *L*/*D* remaining. For flow rates larger than those of the figures, it was also visually observed that the system tended to exhibit slugging. However, in agreement with previous result previously reported in literature, thought the noisy D2 can detect dynamic changes, and it is useful as for the eigenvalues spectra giving a measure of the problem size (dynamic scales), the dynamical link is still unclear.

Kolmogorov entropy

The KE values are shown in Figures 11b and Figure 13). It can be observed that when the bed is operating in bubbling regime, KE gets values close to 6.0. This value is in agreement with the values obtained from the entropy model obtaining by applying the model of Schouten et al. [31] (Figure 13).

$$K\left(\frac{bits}{s}\right)\alpha\frac{\#\ bubble\ eruptions}{s}\cdot bubble\ impact = N\frac{\pi}{4}D_T^2\left(\frac{d_b}{D_T}\right)$$

$$K\left(\frac{bits}{s}\right) = 19.3\cdot\left(u_f - u_{mf}\right)^{0.4}\cdot\left(\frac{D_T}{H_{SB}^{1.6}}\right)$$

The entropy model reported in [31] assumes is linearly proportional to the total number of bubbles that erupt at the total bed surface per unit of time (information loss). The figure 13 compares the result provided by the model using both the Darton et al. [32] and Mori and Wen [33] bubble models. It can be observed that in agreement to the previous result reported in [31] the predicted values for the entropy are higher than the experimental values (figure 13a). In

contrast the model reasonable fits the measured entropies for deeper beds (figure 13c and figure 13d). Consequently, the entropy behaves linearly proportional to the total number of bubbles that erupt at the bed surface. The fact the entropy value could be describe by a simple bubble eruption model as the one described in Schouten et al.[31] confirm that the laterally inspecting bed surface measurement technique used in this research is global. Consequently, it is able to recover the long term dynamic information carried by the erupting bubbles.

Conclusions

The research assumes that bubbling fluidized systems should be considered as a multiphase gas-solid media, where the gas enters, giving rise to bubbles, and exits from. Therefore, the only effective method to measure the long-term behaviour is the volume variation.

The analysis of the periodicity of this variable by using the FFT revealed that for a specified quantity of fluidized material, when the pressure gradient between the plenum and the zero (u_f) increased, the volume oscillation frequency increased marginally; moreover, F_P decreased as weight increased.

Occasionally, two F_P appeared, which could be interpreted considering the extremes of the range of variables studied: a) At the lower end of the weight range, i.e., at low L/D, the volume change by the bubble entry is expressed by a second main frequency and b) at the end of the interval corresponding to high L/D and low u_f, another second main frequency indicates that slugging begins to occur.

That the attractor could be constructed and its properties measured verify that the dynamics of a few of the phenomena assumed when the model was assumed to be “chaotic”. It is reasonable to consider that the nonlinear dynamics corresponds to the growth of bubbles by adiabatic decompression. Thus, the singular value decomposition establishes that there were between 4 and 6 independent variables, dynamical scales, in which most of the information was concentrated.

The evolution of the attractors’ geometry with the variation in u_f and W verifies the effect of both. This fact has been indicated in Figure 10, where the results for the projections in the 2D plane are presented; it also occurs for the 3D projections in Figures 8 and 9. Thus, the change in appearance of the attractor would represent that the expansion velocity of the bubbles that are closest to the distributor gas is low when the pressure exerted by the bed is high, and vice versa.

The entropy value behaves linearly proportional to the total number of bubbles that erupt at the bed surface and could be described by the bubble eruption model, which confirms that the laterally inspecting bed surface measurement technique used in this research is global. The close relationship between the eruption of bubbles and the behaviour of the fluidized bed system emphasize the role of the pressure gradient existing between the plenum and the bed surface for the understanding of the dynamics of gas/solid fluidized beds.

Acknowledgements

Funding: This research was funded by the Spanish Ministry of Research through Project CTQ2006-15525-C02-02.

Notation

d_b = bubble diameter, cm

d_{b0} = bubble diameter immediately above gas distributor, cm

d_p = particle diameter, µm

F_p = principal frequency in the power spectra, Hz

FB = fluidized bed

H_{SB} = static bed height, cm

h = pattern height to examine flatness of the bed surface, µm

k = eigenvalue index, (-)

L/D = height/width ratio of the bed, (-)

$P_{op\text{-}comp}$ = operation pressure of compressor, Pa

u_b = bubble velocity, cm/s

u_f = velocity fluidization, cm/s

u_{mf} = minimum fluidization velocity, m/s

w = pattern width to examine flatness of the bed surface, µm

Greek symbols

Δp = pressure drop across fluidized bed, Pa

$\Delta p_{g\text{-}or}$ = pressure drop across a distributor orifice, Pa

μ_f = gas viscosity, kg/m/s

ρ_b = bubble density in the bed, nº bubbles/m^3

ρ_f = gas density, kg/m^3

ρ_p = particle density, kg/m^3

ρ_{si} = density gas exchange surface, m^2/m^3

Literature Cited

[1] LIRAG, R.C. and LITTMAN, H., 1971. Statistical Study of the Pressure Fluctuations in a Fluidized Bed. AIChE Symposium Series, nº 116, vol. 67, no. nº 116, pp. 11.

[2] FAN, L., HO, T., HIRAOKA, S. and WALAWENDER, W., 1981. Pressure-Fluctuations in a Fluidized-Bed. AIChE Journal, vol. 27, no. 3, pp. 388-396 ISSN 0001-1541. DOI 10.1002/aic.690270308.

[3] CHEREMISINOFF, N., 1986. Review of Experimental Methods for Studying the Hydrodynamics of Gas Solid Fluidized-Beds. Industrial & Engineering Chemistry Process Design and Development, APR, vol. 25, no. 2, pp. 329-351 ISSN 0196-4305. DOI 10.1021/i200033a001.

[4] GELDART, D., 1987. Gas Fluidization Technology. D. GELDART ed., Chichester: John Wiley & Sons ISBN 0 471 90806 1.

[5] WERTHER, J., 1999. Measurement techniques in fluidized beds. Powder Technology, APR, vol. 102, no. 1, pp. 15-36 ISSN 0032-5910. DOI 10.1016/S0032-5910(98)00202-2

[6] VAN OMMEN, J.R. and MUDDE, R.F., 2008. Measuring the Gas-Solids Distribution in Fluidized Beds-A Review. International Journal of Chemical Reactor Engineering, vol. 6, pp. R3 ISSN 2194-5748.

[7] AGHBASHLO, M., SOTUDEH-GHAREBAGH, R., ZARGHAMI, R., MUJUMDAR, A.S. and MOSTOUFI, N., 2014. Measurement Techniques to Monitor and Control Fluidization Quality in Fluidized Bed Dryers: A Review. Drying Technology, vol. 32, no. 9, pp. 1005-1051 ISSN 0737-3937. DOI 10.1080/07373937.2014.899250.

[8] SUN, J. and YAN, Y., 2016. Non-intrusive measurement and hydrodynamics characterization of gas-solid fluidized beds: a review. Measurement Science and Technology, NOV, vol. 27, no. 11, pp. 112001 ISSN 0957-0233. DOI 10.1088/0957-0233/27/11/112001.

[9] GUARDIOLA, J., ARAGON, J.M., RAMOS, G., ELVIRA, R. and MARTIN, D., 2012. Interface sensor based on computer vision: Fine tuning using a fluidized bed. AIChE Journal, DEC, vol. 58, no. 12, pp. 3645-3652 ISSN 0001-1541. DOI 10.1002/aic.13756.

[10] GUARDIOLA, J., RAMOS, G. and ELVIRA, R., 2013. Measuring the height of a fluidized bed by computer vision. Chemical Engineering Science, MAY 24, vol. 95, pp. 33-42 ISSN 0009-2509. DOI 10.1016/j.ces.2013.03.008.

[11] DHODAPKAR, S. and KLINZING, G., 1993. Pressure Fluctuation Analysis for a Fluidized-Bed. Weimer, AW Chen, JC Fan, LS Yang,WC ed., ISBN 0-8169-0617-3.

[12] SVENSSON, A., JOHNSSON, F. and LECKNER, B., 1996. Fluidization regimes in non-slugging fluidized beds: The influence of pressure drop across the air distributor. Powder Technology, MAR, vol. 86, no. 3, pp. 299-312 ISSN 0032-5910. DOI 10.1016/0032-5910(95)03055-7.

[13] VAN DER SCHAAF, J., SCHOUTEN, J. and VAN DEN BLEEK, C., 1998. Decomposition of power spectral density of pressure fluctuations in gas-solids fluidized beds. 3rd International Conference on Multiphase Flow (ICMF '98).

[14] VAN DER SCHAAF, J., SCHOUTEN, J., JOHNSSON, F. and VAN DEN BLEEK, C., 2002. Non-intrusive determination of bubble and slug length scales in fluidized beds by decomposition of the power spectral density of pressure time series. International Journal of Multiphase Flow, MAY, vol. 28, no. 5, pp. 865-880 ISSN 0301-9322. DOI 10.1016/S0301-9322(01)00090-8.

[15] TRNKA, O., VESELY, V., HARTMAN, M. and BERAN, Z., 2000. Identification of the state of a fluidized bed by pressure fluctuations. AIChE Journal, MAR, vol. 46, no. 3, pp. 509-514 ISSN 0001-1541. DOI 10.1002/aic.690460309.

[16] VAN WACHEM, B., SCHOUTEN, J., KRISHNA, R. and VAN DEN BLEEK, C., 1999. Validation of the Eulerian simulated dynamic behaviour of gas-solid fluidised beds. Chemical

Engineering Science, JUL, vol. 54, no. 13-14, pp. 2141-2149 ISSN 0009-2509. DOI 10.1016/S0009-2509(98)00303-0.

[17] VAN OMMEN, J.R., SASIC, S., VAN DER SCHAAF, J., GHEORGHIU, S., JOHNSSON, F. and COPPENS, M., 2011. Time-series analysis of pressure fluctuations in gas-solid fluidized beds - A review. International Journal of Multiphase Flow, JUN, vol. 37, no. 5, pp. 403-428 ISSN 0301-9322. DOI 10.1016/j.ijmultiphaseflow.2010.12.007.

[18] SVOBODA, K., CERMAK, J., HARTMAN, M., DRAHOS, J. and SELUCKY, K., 1983. Pressure-Fluctuations in Gas-Fluidized Beds at Elevated-Temperatures. Industrial & Engineering Chemistry Process Design and Development, vol. 22, no. 3, pp. 514-520 ISSN 0196-4305. DOI 10.1021/i200022a029.

[19] VAN OMMEN, J., COPPENS, M., VAN DEN BLEEK, C. and SCHOUTEN, J., 2000. Early warning of agglomeration in fluidized beds by attractor comparison. AIChE Journal, NOV, vol. 46, no. 11, pp. 2183-2197 ISSN 0001-1541. DOI 10.1002/aic.690461111.

[20] SCHOUTEN, J., ZIJERVELD, R. and VAN DEN BLEEK, C., 1999. Scale-up of bottom-bed dynamics and axial solids-distribution in circulating fluidized beds of Geldart-B particles. Chemical Engineering Science, JUL, vol. 54, no. 13-14, pp. 2103-2112 ISSN 0009-2509. DOI 10.1016/S0009-2509(98)00352-2.

[21] GRASSBERGER, P. and PROCACCIA, I., 1983b. Measuring the Strangeness of Strange Attractors. Physica D, vol. 9, no. 1-2, pp. 189-208 ISSN 0167-2789. DOI 10.1016/0167-2789(83)90298-1.

[22] SCHOUTEN, J., TAKENS, F. and VANDENBLEEK, C., 1994a. Estimation of the Dimension of a Noisy Attractor. Physical Review E, SEP, vol. 50, no. 3, pp. 1851-1861 ISSN 1063-651X. DOI 10.1103/PhysRevE.50.1851.

[23] ELLNER, S., 1988. Estimating Attractor Dimensions from Limited Data - a New Method, with Error-Estimates. Physics Letters a, NOV 7, vol. 133, no. 3, pp. 128-133 ISSN 0375-9601. DOI 10.1016/0375-9601(88)90772-4.

[24] ABARBANEL, H., BROWN, R., SIDOROWICH, J. and TSIMRING, L., 1993. The Analysis of Observed Chaotic Data in Physical Systems. Reviews of Modern Physics, OCT, vol. 65, no. 4, pp. 1331-1392 ISSN 0034-6861. DOI 10.1103/RevModPhys.65.1331.

[25] ECKMANN, J. and RUELLE, D., 1985. Ergodic-Theory of Chaos and Strange Attractors. Reviews of Modern Physics, vol. 57, no. 3, pp. 617-656 ISSN 0034-6861. DOI 10.1103/RevModPhys.57.617.

[26] DAW, C. and HALOW, J., 1993. Evaluation and Control of Fluidization Quality through Chaotic Time-Series Analysis of Pressure-Drop Measurements. Weimer, AW Chen, JC Fan, LS Yang,WC ed., ISBN 0-8169-0617-3.

[27] GRASSBERGER, P. and PROCACCIA, I., 1983a. Estimation of the Kolmogorov-Entropy from a Chaotic Signal. Physical Review a, vol. 28, no. 4, pp. 2591-2593 ISSN 1050-2947. DOI 10.1103/PhysRevA.28.2591.

[28] SCHOUTEN, J., TAKENS, F. and VANDENBLEEK, C., 1994b. Maximum-Likelihood-Estimation of the Entropy of an Attractor. Physical Review E, JAN, vol. 49, no. 1, pp. 126-129 ISSN 1063-651X. DOI 10.1103/PhysRevE.49.126. TOOMEY, R. and JOHNSTONE, H., 1952. Gaseous Fluidization of Solid Particles. Chemical Engineering Progress, vol. 48, no. 5, pp. 220-226 ISSN 0360-7275.

[29] KAGE, H., IWASAKI, N., YAMAGUCHI, H. and MATSUNO, Y., 1991. Frequency-Analysis of Pressure Fluctuation in Fluidized-Bed Plenum. Journal of Chemical Engineering of Japan, FEB, vol. 24, no. 1, pp. 76-81 ISSN 0021-9592. DOI 10.1252/jcej.24.76.

[30] KAGE, H., AGARI, M., OGURA, H. and MATSUNO, Y., 2000. Frequency analysis of pressure fluctuation in fluidized bed plenum and its confidence limit for detection of various modes of fluidization. Advanced Powder Technology, vol. 11, no. 4, pp. 459-475 ISSN 0921-8831. DOI 10.1163/156855200750172060.

[31] SCHOUTEN, J.C. , VANDER STAPPEN, M.L.M., and VAN DEN BLEEK, C.M, 1996. Scale-up of chaotic fluidized bed hydrodynamics. Chemical Engineering Science, MAY, Vol. 51, No. 10, pp. 1991-2000.

[32] DARTON, R.C., LANAUZE, R.D., DAVIDSON, J.F., HARRISON, D., 1977. Bubble growth due to coalescence in fluidised beds. Trans Inst Chem Eng 55, 274-280.

[33] MORI, S., WEN, C.Y., 1975. Estimation of bubble diameter in gaseous fluidized beds. AIChE J. 21, 109-115.

Figure 1. Experimental set up used to monitor changes in bed height.

Figure 2: Effect of fluidization gas flow on fluctuation of bed volume. a) W = 1.020 kg, u_f = 0.475 m/s, left vertical axis; b) W = 1.020 kg, u_f = 0.555 m/s, left vertical axis; c) W = 1.567 kg, u_f = 0.454 m/s, right vertical axis; d) W = 1.567 kg, u_f = 0.490 m/s, right vertical axis.

Figure 3: Effect of weight of fluidized material on variation in bed volume. a) W = 1.020 kg, u_f = 0.475 m/s; b) W = 1.219 kg, u_f = 0.478 m/s; c) W = 1.393 kg, u_f = 0.478 m/s; d) W = 1.567 kg, u_f = 0.478 m/s.

Figure 4. Fourier power spectra of superficial oscillation of bed surface at three selected fluidizing conditions: (a) H_{SB} = 233.76 mm, u_f = 0.527 cm/s, F_p = 1.53 Hz; (b) H_{SB} = 347.25 mm, u_f = 0.489 cm/s, F_p = 1.09 Hz; (c) H_{SB} = 443.70 mm, u_f = 0.466 cm/s, F_p = 0.65 Hz.

Figure 5: Effects of weight and gas flow on bed volume oscillation.

Figure 6. Eigenvalues spectra for experiments with several gas flow values. W = 0.816 kg, H_{SB} = 233.78 mm. (a): u_f = 0.4413 cm/s; (b): u_f = 0.4750 cm/s; (c): u_f = 0.5271 cm/s; (d): u_f = 0.5639 cm/s.

Figure 7. Eigenvalue spectra for experiments with several values of quantity of fluidized material. (a): H_{SB} = 292.87 mm, u_f = 0.4750 cm/s; (b): H_{SB} = 347.25 mm, u_f = 0.4781 cm/s; (c): H_{SB} = 395.28 mm, u_f = 0.4781 cm/s; (d): H_{SB} = 443.70 mm, u_f = 0.4781 cm/s.

Figure 8. Attractors when bed height varies over time. W = 1.219 kg, H_{SB} = 347.25 mm, (a): u_f = 0.4413 cm/s; (b): u_f = 0.4535 cm/s; (c): u_f = 0.4658 cm/s; (d): u_f = 0.4781 cm/s; (e): u_f = 0.4891 cm/s.

Figure 9. Attractors when bed height varies over time. W = 1.567 kg, H_{SB} = 443.70 mm, (a): u_f = 0.4413 cm/s; (b): u_f = 0.4535 cm/s; (c): u_f = 0.4658 cm/s; (d): u_f = 0.4781 cm/s; (e): u_f = 0.4903 cm/s.

Figure 10. Relationship between main components of attractors. (a)–(b): W = 0.816 kg, H_{SB} = 233.78 mm, u_f = 0.4658 cm/s; (c)–(d): W = 1.020 kg, H_{SB} = 292.87 mm, u_f = 0.4750 cm/s; (e)–(f): W = 1.393 kg, H_{SB} = 395.28 mm, u_f = 0.4781 cm/s.

Figure 11. Effect of u_f on D_2 and KE. W = 0.816 kg, H_{SB} = 233.78 mm.

Figure 12. Influence of variables studied on D_2. (a): H_0 = 292.87 mm; (b) H_0 = 347.25 mm; (c): H_{SB} = 395.28 mm; (d) H_0 = 443.70 mm.

Figure 13. Effect of variables studied on KE. (a): H_0 = 292.87 mm; (b) H_0 = 347.25 mm; (c): H_{SB} = 395.28 mm; (d) H_0 = 443.70 mm.

Table 1. Quantities of fluidized material and fluidization velocities.

Table 1. Cantidades de material fluidizado y velocidades de fluidización

W, kg	H_0, mm	u_{mf}. m/s
0,816	233,78	0,441 - 0,564
1,020	292,87	
1,219	347,25	0,441 - 0,492
1,393	395,28	
1,567	443,70	

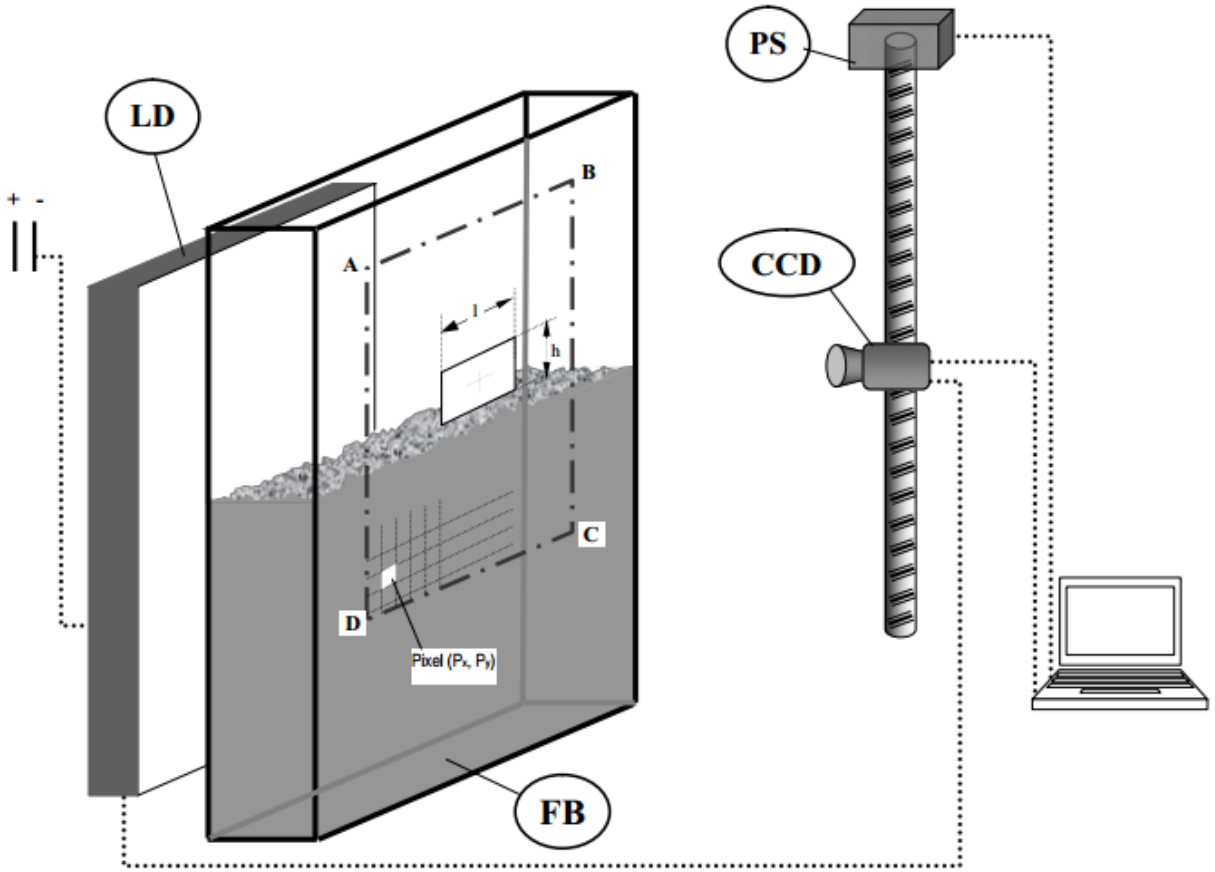

Figure 1

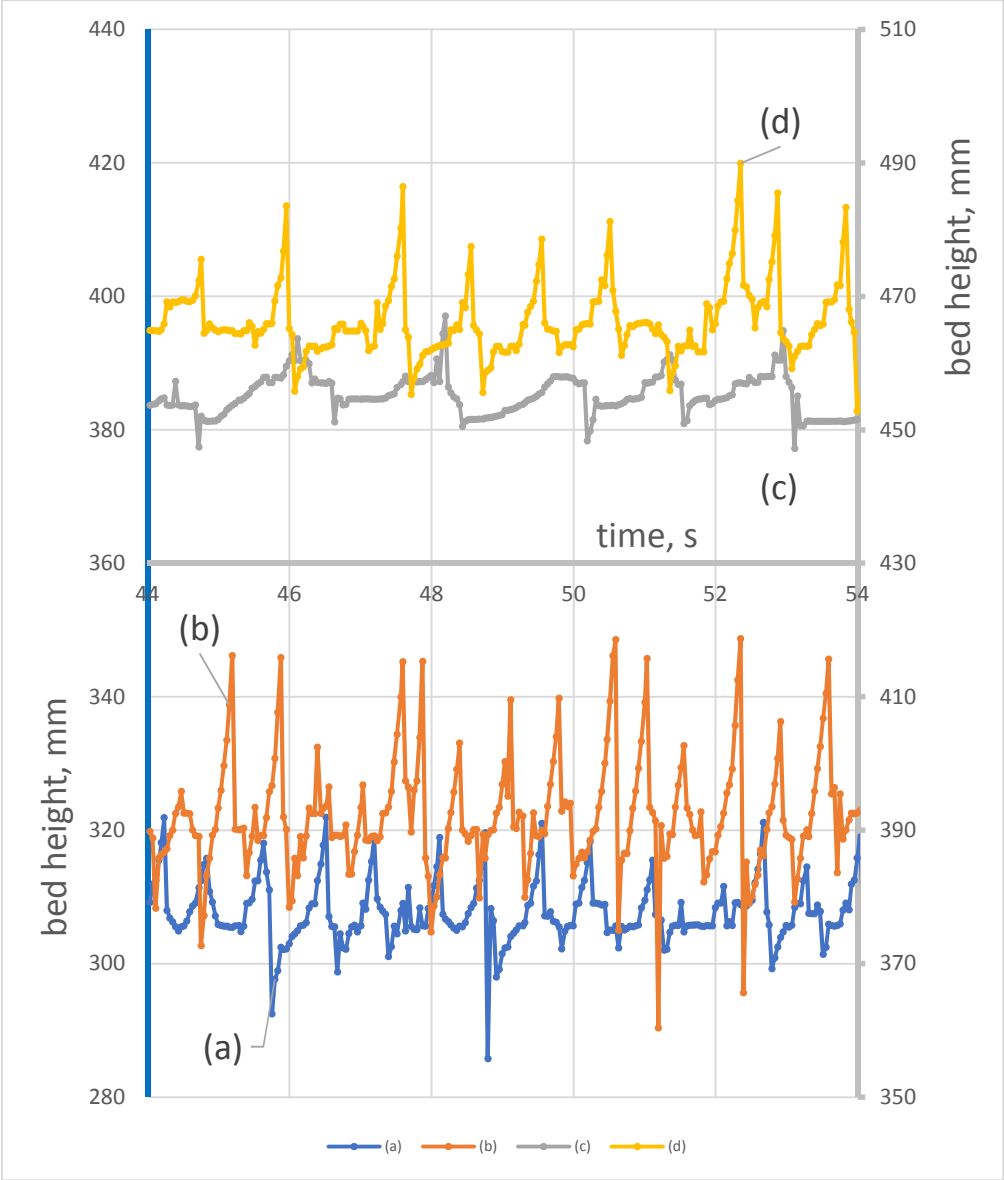
440
420
400
380
360
510
490
470
450
430
bed height, mm
(d)
(c)
time, s
44
46
48
50
52
54
(b)
(a)
340
320
300
280
410
390
370
350
bed height, mm
(a)
(b)
(c)
(d)

Figure 2

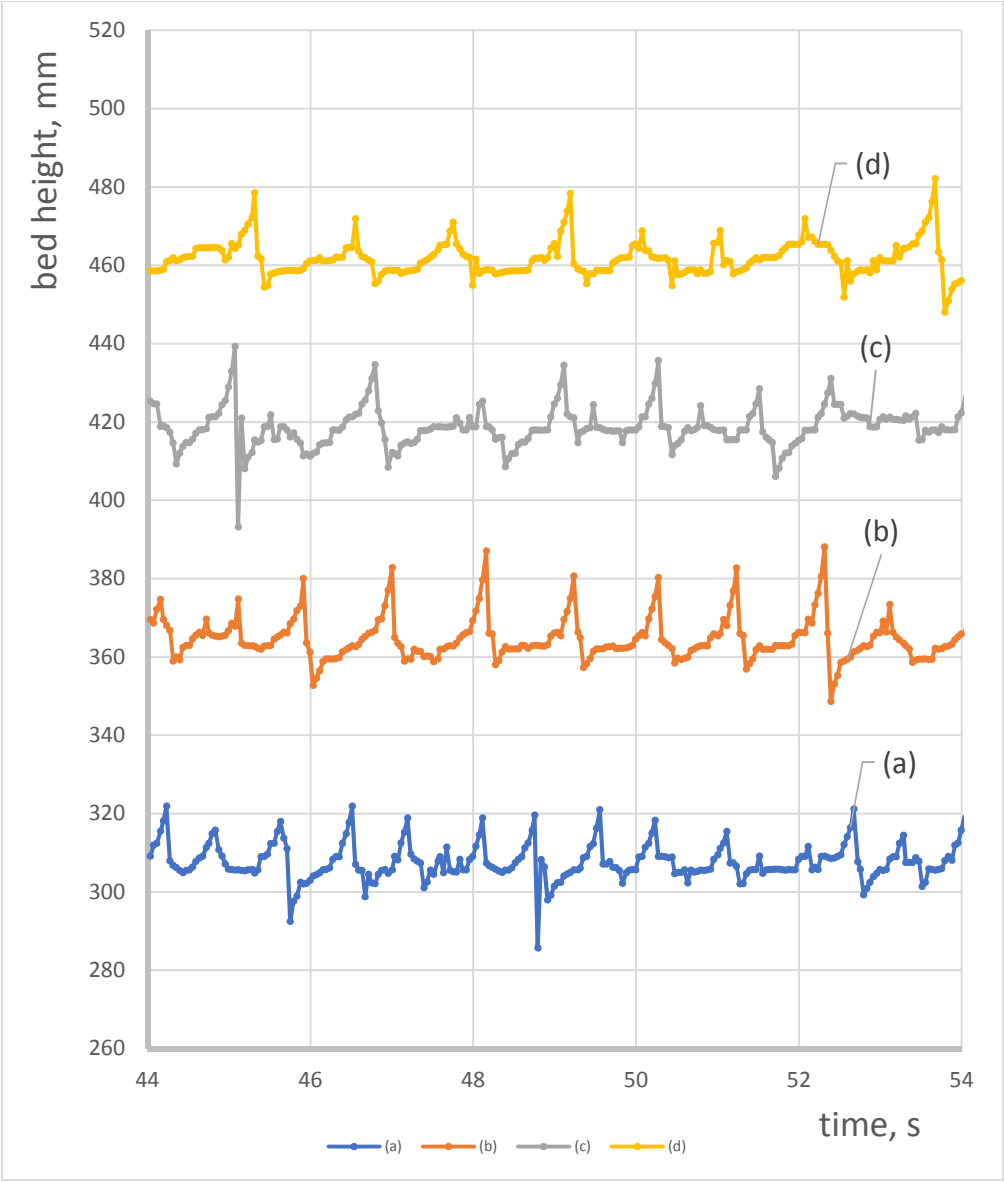
bed height, mm
520
500
480
460
440
420
400
380
360
340
320
300
280
260
44
46
48
50
52
54
time, s
(a)
(b)
(c)
(d)
(a)
(b)
(c)
(d)

Figure 3

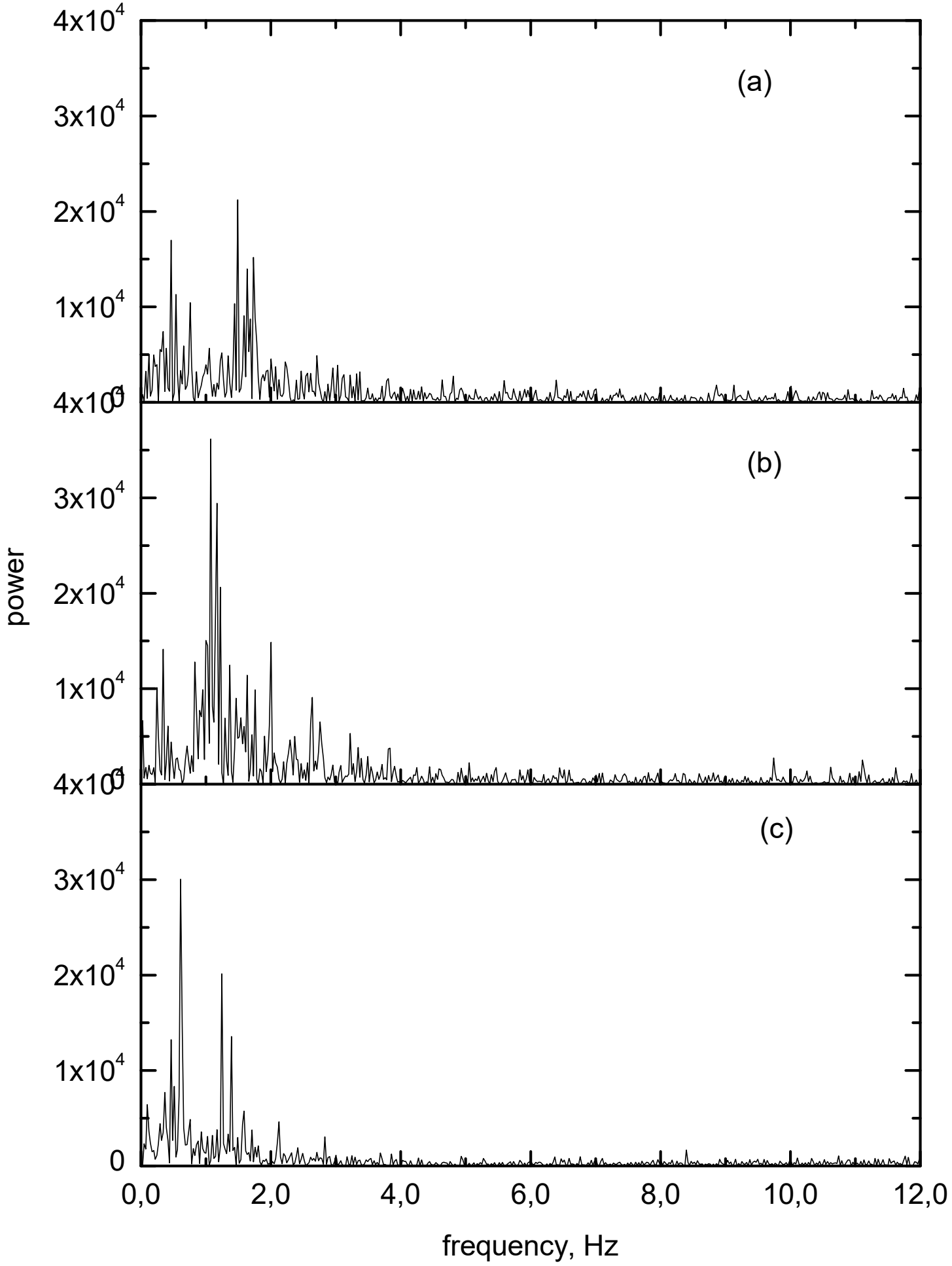
4x10^4
3x10^4
2x10^4
1x10^4
0
(a)
(b)
(c)
power
0,0
2,0
4,0
6,0
8,0
10,0
12,0
frequency, Hz

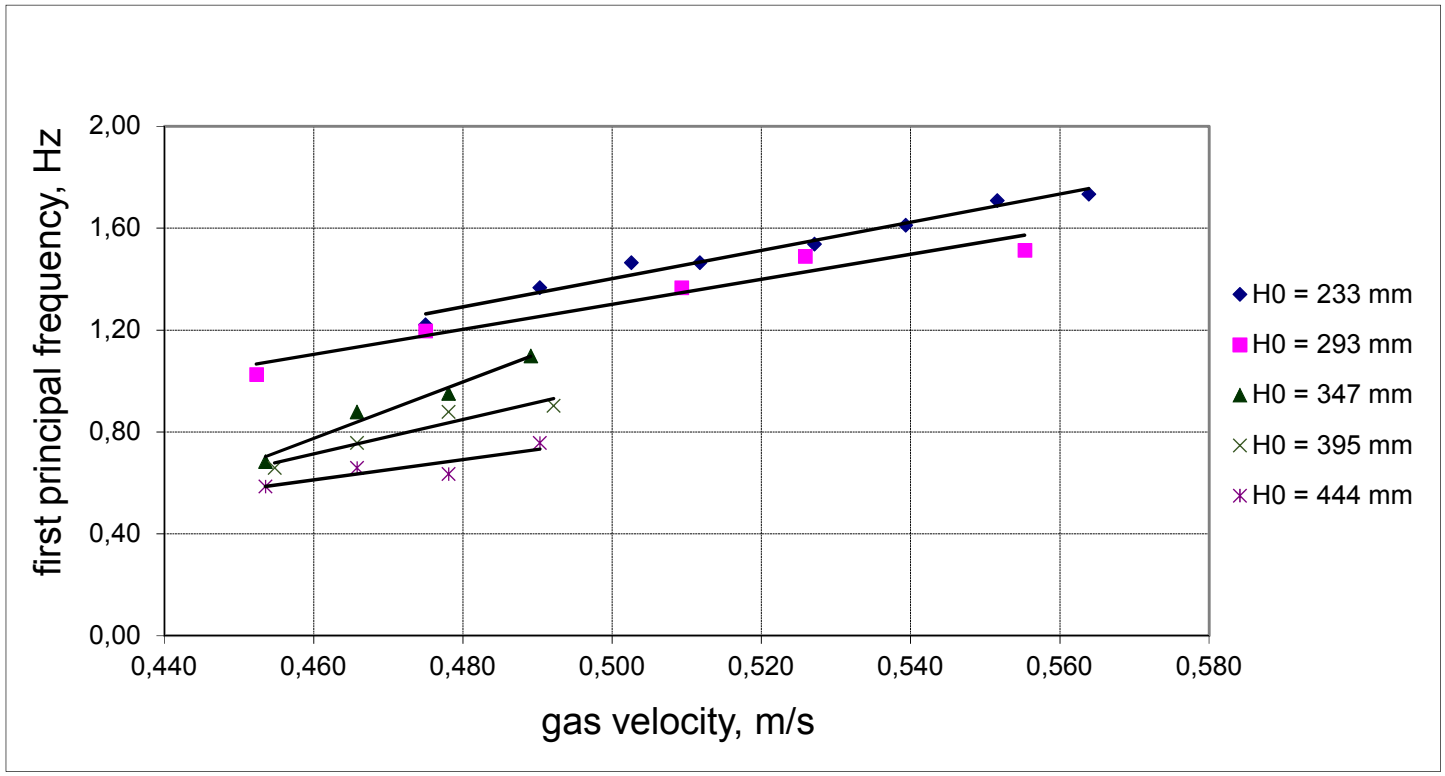
first principal frequency, Hz
2,00
1,60
1,20
0,80
0,40
0,00
0,440
0,460
0,480
0,500
0,520
0,540
0,560
0,580
gas velocity, m/s
H0 = 233 mm
H0 = 293 mm
H0 = 347 mm
H0 = 395 mm
H0 = 444 mm

Figure 5

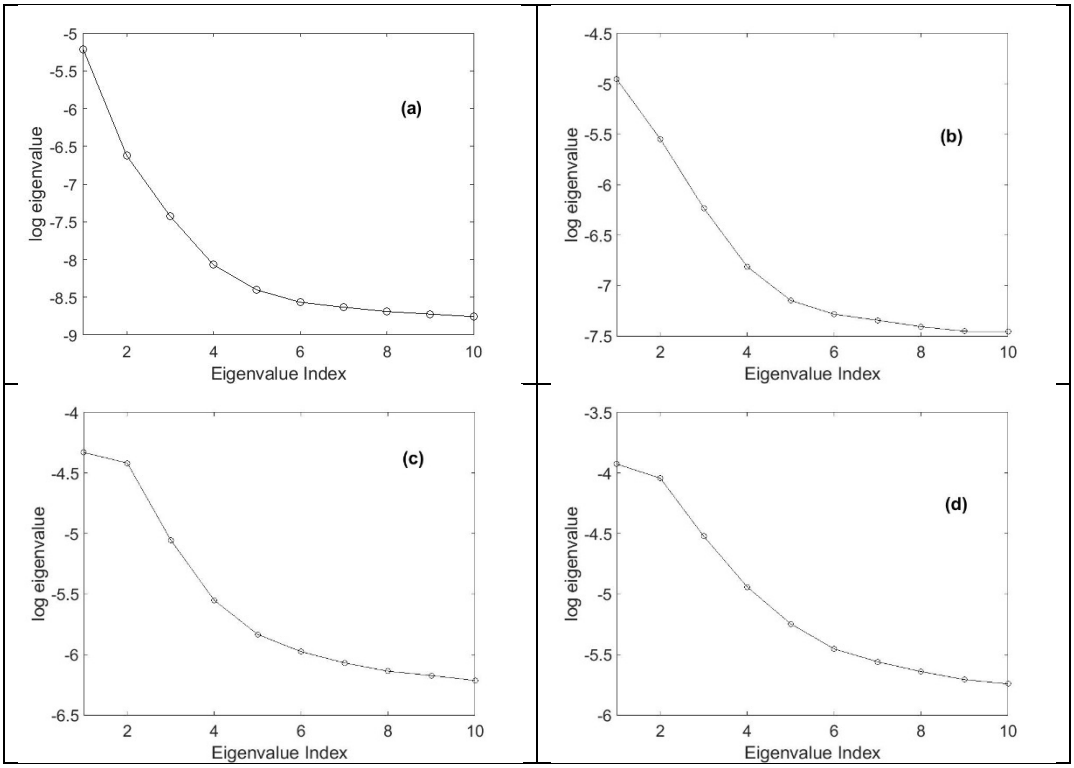
(a)
log eigenvalue
Eigenvalue Index
(b)
log eigenvalue
Eigenvalue Index
(c)
log eigenvalue
Eigenvalue Index
(d)
log eigenvalue
Eigenvalue Index

Figure 6

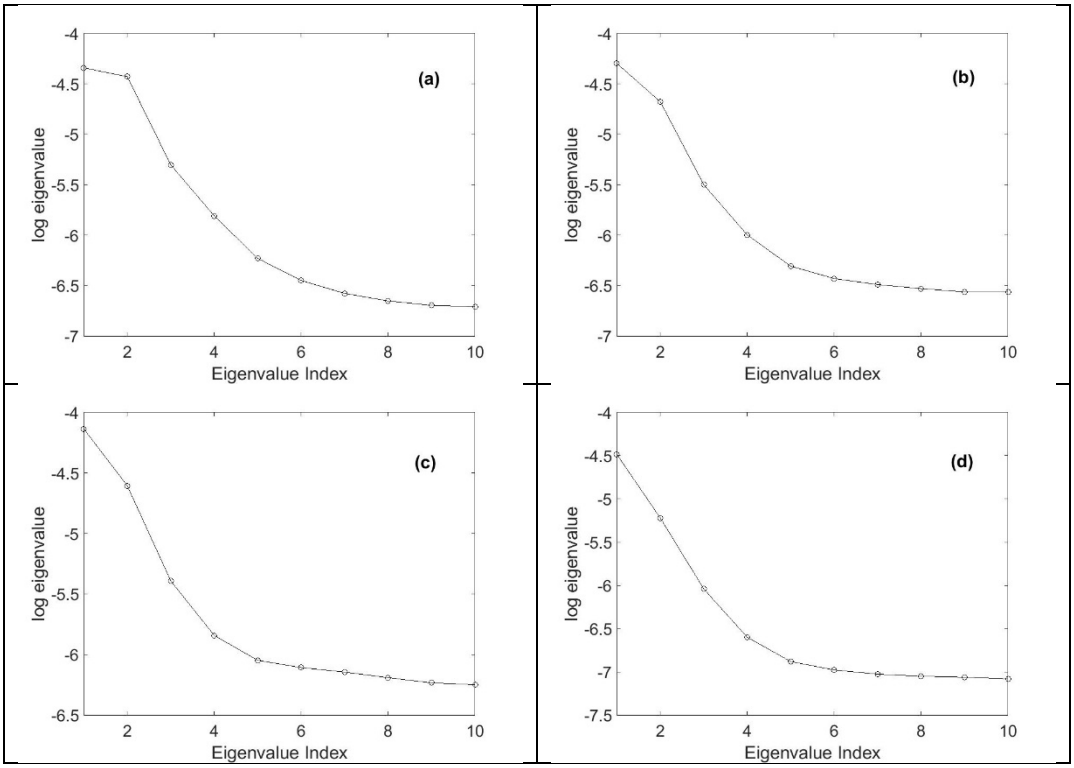

Figure 7

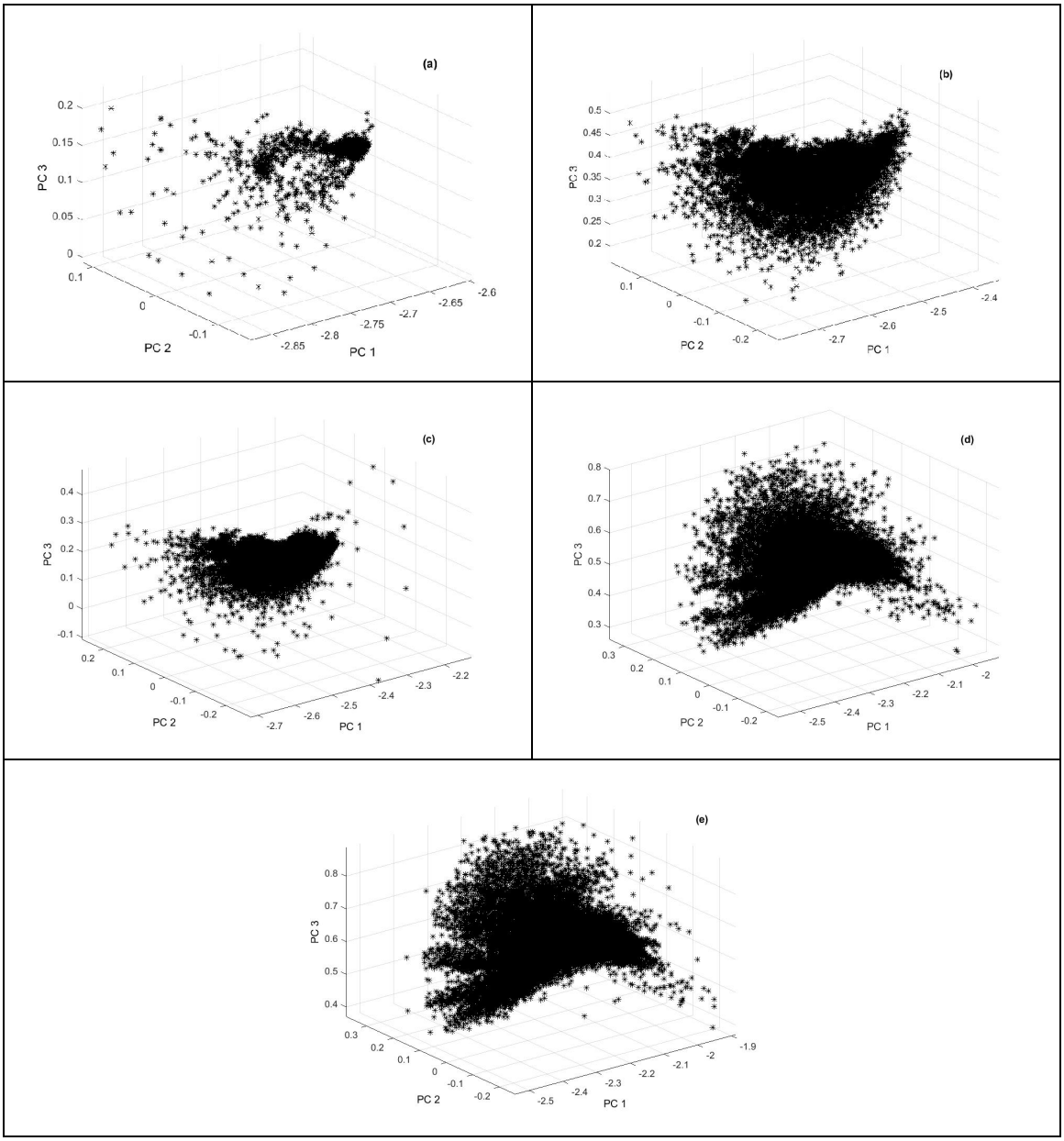
(a)
PC 3
PC 2
PC 1
(b)
PC 3
PC 2
PC 1
(c)
PC 3
PC 2
PC 1
(d)
PC 3
PC 2
PC 1
(e)
PC 3
PC 2
PC 1

Figure 8

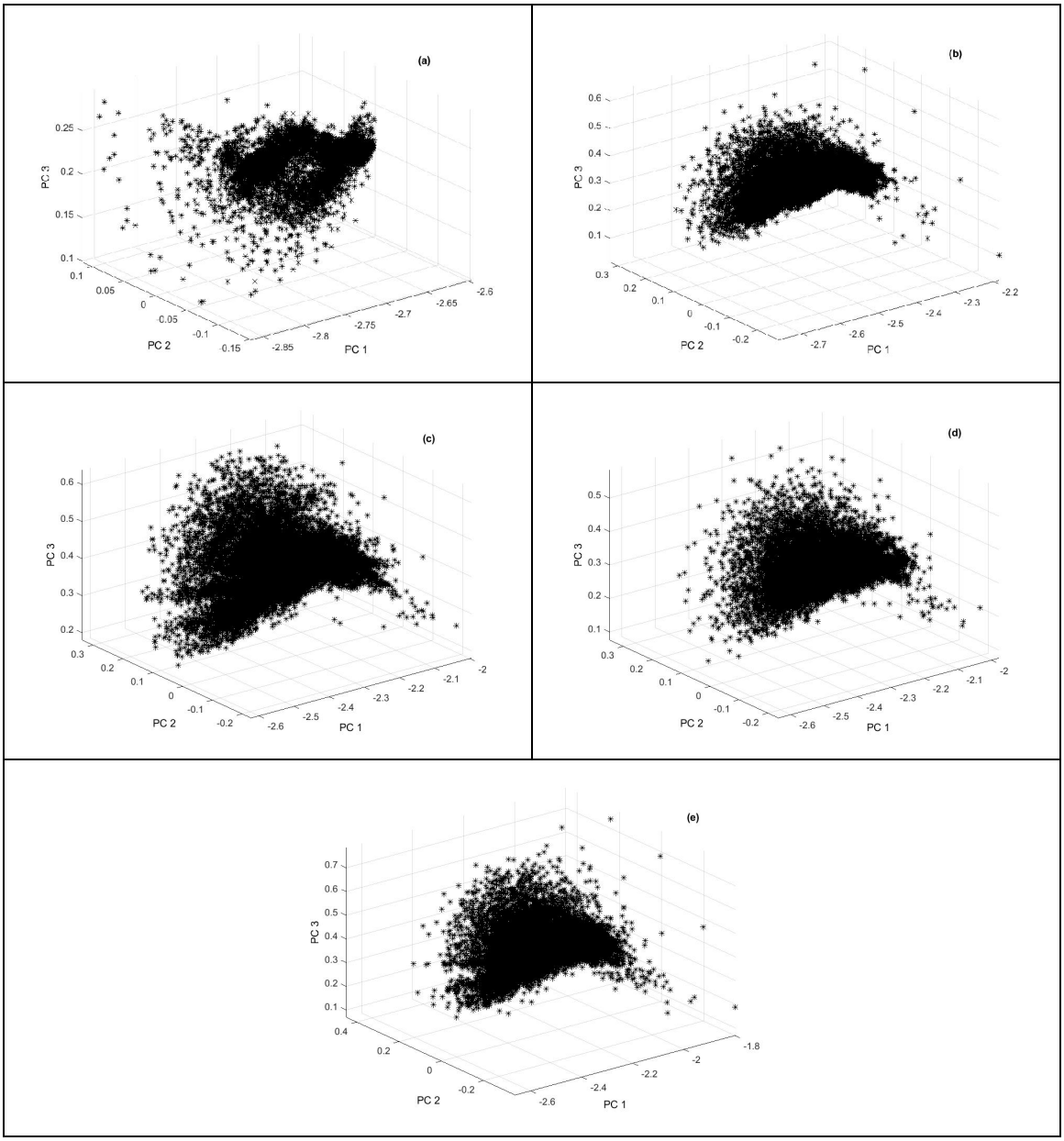
(a)
PC 3
PC 2
PC 1
(b)
PC 3
PC 2
PC 1
(c)
PC 3
PC 2
PC 1
(d)
PC 3
PC 2
PC 1
(e)
PC 3
PC 2
PC 1

Figure 9

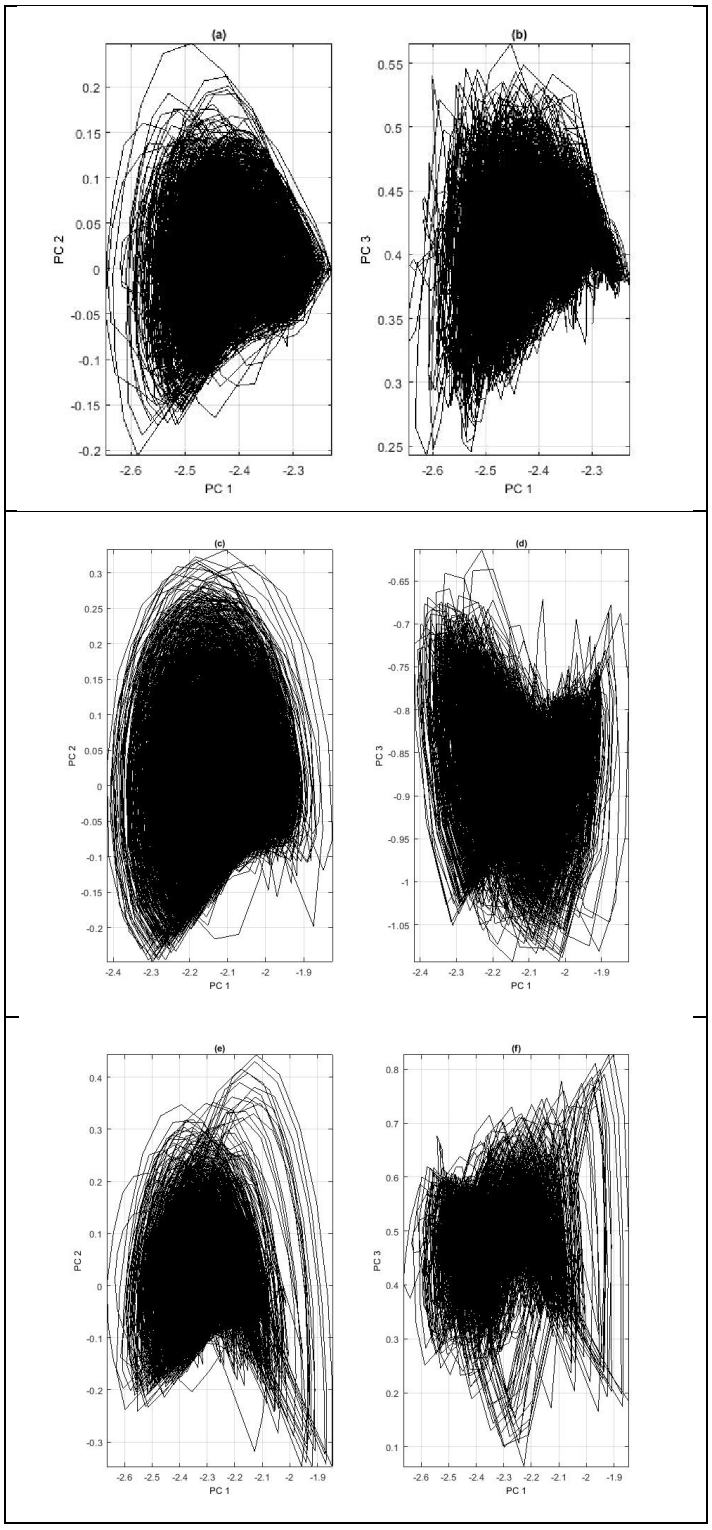

Figure 10

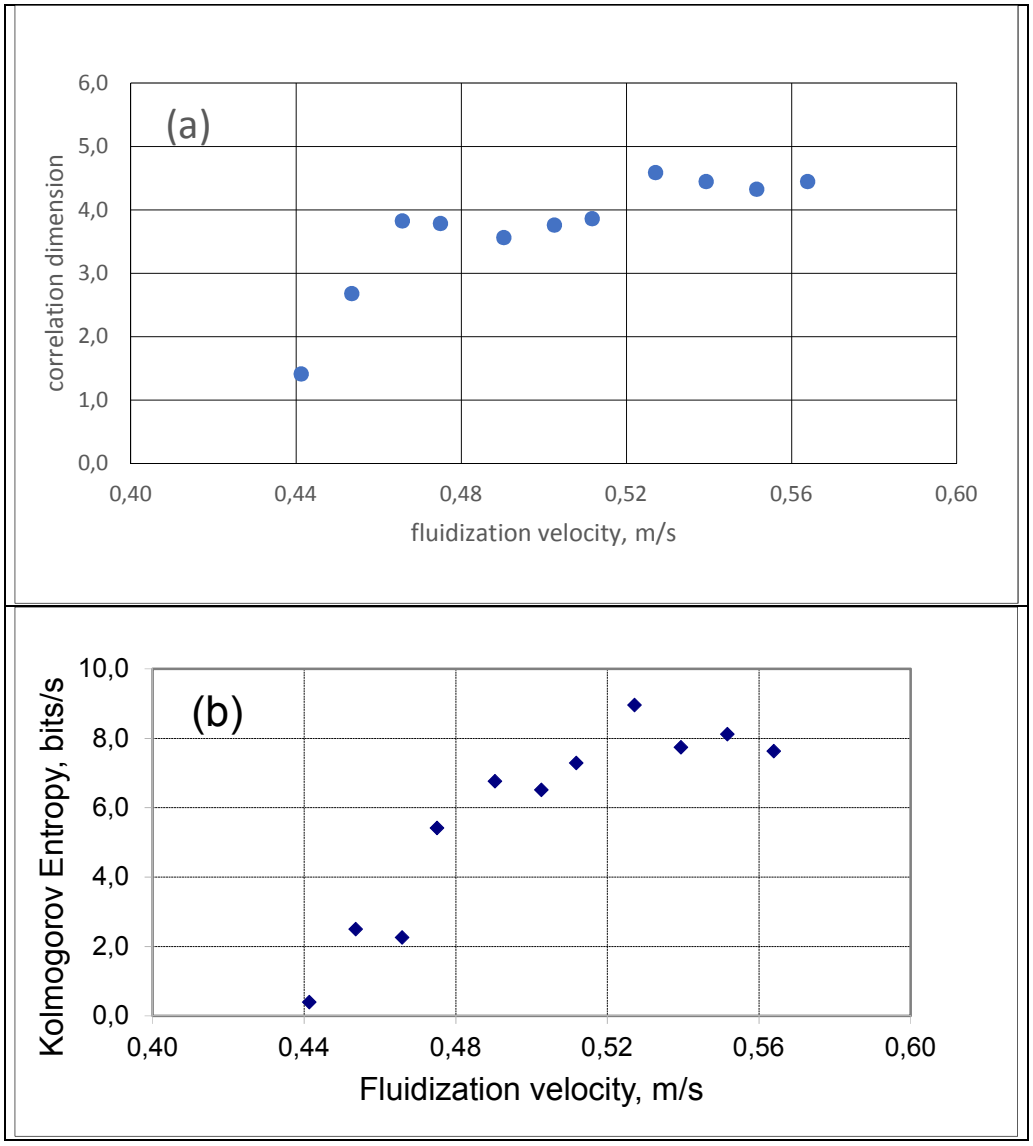
(a)
correlation dimension
6,0
5,0
4,0
3,0
2,0
1,0
0,0
0,40
0,44
0,48
0,52
0,56
0,60
fluidization velocity, m/s
(b)
Kolmogorov Entropy, bits/s
10,0
8,0
6,0
4,0
2,0
0,0
0,40
0,44
0,48
0,52
0,56
0,60
Fluidization velocity, m/s

Figure 11

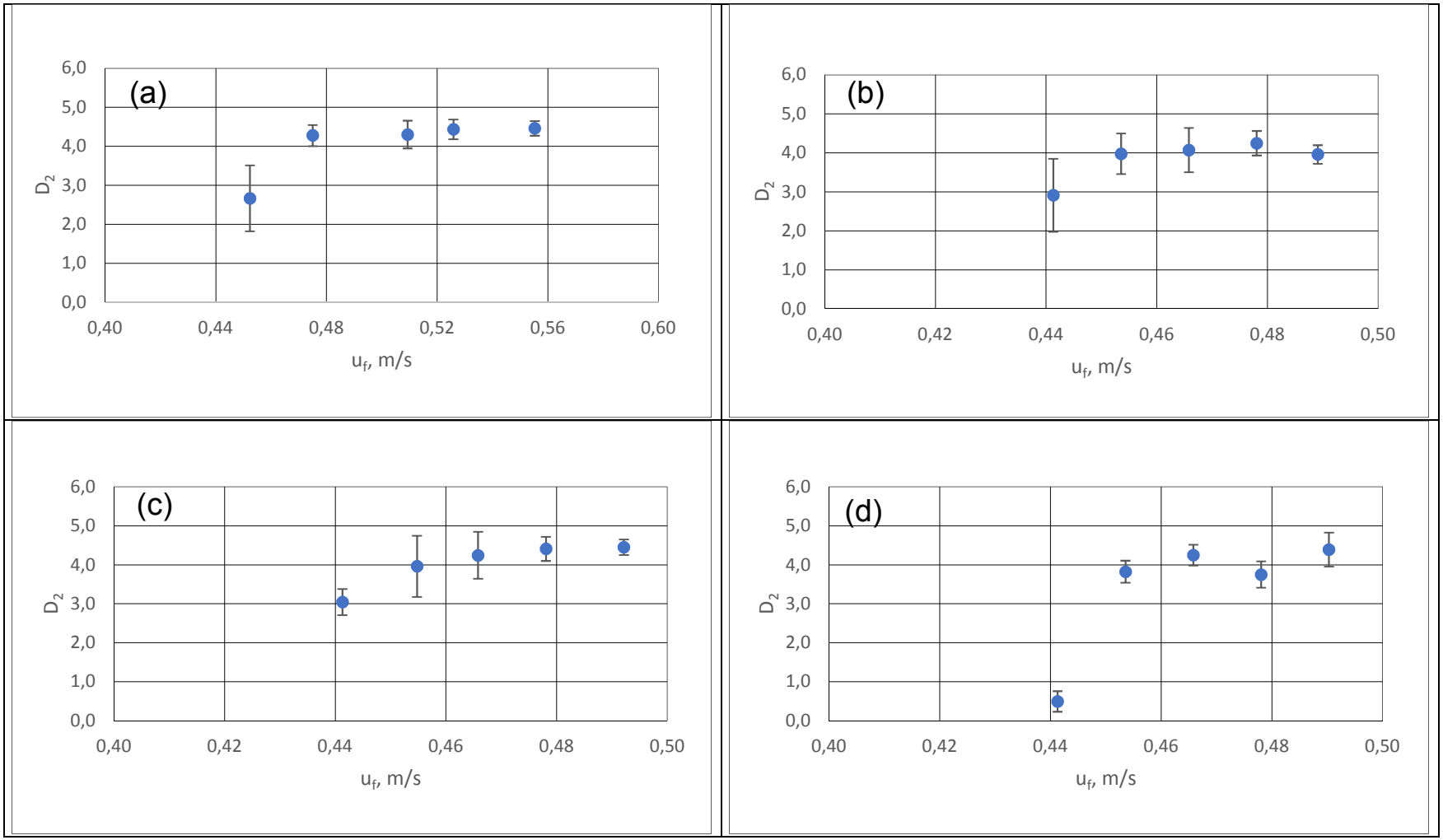
(a)
6,0
5,0
4,0
3,0
2,0
1,0
0,0
D2
0,40
0,44
0,48
0,52
0,56
0,60
uf, m/s
(b)
6,0
5,0
4,0
3,0
2,0
1,0
0,0
D2
0,40
0,42
0,44
0,46
0,48
0,50
uf, m/s
(c)
6,0
5,0
4,0
3,0
2,0
1,0
0,0
D2
0,40
0,42
0,44
0,46
0,48
0,50
uf, m/s
(d)
6,0
5,0
4,0
3,0
2,0
1,0
0,0
D2
0,40
0,42
0,44
0,46
0,48
0,50
uf, m/s

Figure 12

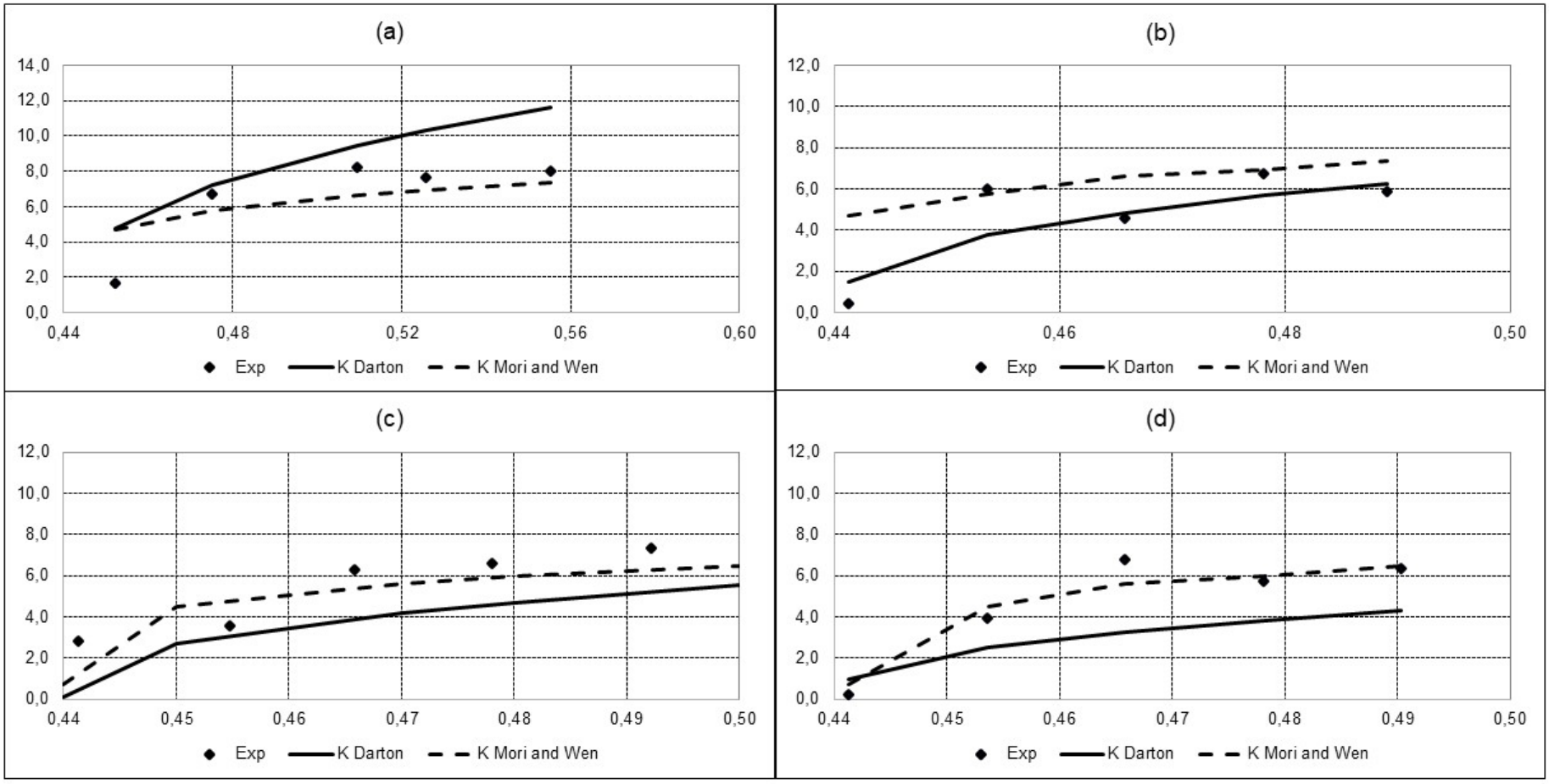
(a)
14,0
12,0
10,0
8,0
6,0
4,0
2,0
0,0
0,44
0,48
0,52
0,56
0,60
Exp
K Darton
K Mori and Wen
(b)
12,0
10,0
8,0
6,0
4,0
2,0
0,0
0,44
0,46
0,48
0,50
Exp
K Darton
K Mori and Wen
(c)
12,0
10,0
8,0
6,0
4,0
2,0
0,0
0,44
0,45
0,46
0,47
0,48
0,49
0,50
Exp
K Darton
K Mori and Wen
(d)
12,0
10,0
8,0
6,0
4,0
2,0
0,0
0,44
0,45
0,46
0,47
0,48
0,49
0,50
Exp
K Darton
K Mori and Wen